



ORIGINAL ARTICLE

Synthesis and characterization of N-doped TiO₂ and its enhanced visible-light photocatalytic activity



Xiuwen Cheng^{a,b,c}, Xiujuan Yu^{a,b,*}, Zipeng Xing^{a,b}, Lisha Yang^{a,b}

^a Department of Environmental Science and Engineering, Heilongjiang University, Xuefu Road 74, Nangang District, Harbin 150080, PR China

^b Key Laboratory of Chemical Engineering Process & Technology for High-Efficiency Conversion, College of Heilongjiang Province, Harbin, PR China

^c State Key Laboratory of Urban Water Resources and Environment (SKLUWRE), Department of Environmental Science and Engineering, Harbin Institute of Technology, Huanghe Road 73, Nangang District, Harbin 150090, PR China

Received 28 December 2011; accepted 27 April 2012

Available online 9 May 2012

KEYWORDS

N doped;
TiO₂;
Visible light;
Photocatalysis;
RhB

Abstract Nitrogen doped titanium dioxide (N-TiO₂) nano-photocatalysts were successfully synthesized in the presence of ammonium chloride. The resulting materials were characterized by X-ray diffraction (XRD), transmission electron microscopy (TEM), scanning electron microscopy (SEM), X-ray photoelectron spectroscopy (XPS), Fourier transform infrared spectroscopy (FTIR) and ultraviolet–visible diffuse reflection spectroscopy (UV–vis DRS). The results of XRD, SEM and TEM revealed that the as-synthesized photocatalyst was composed of spheroidal particles, which were smaller than undoped ones. XPS analysis revealed that N was effectively incorporated into the lattice of TiO₂ through substituting oxygen atoms, and N might coexist in the form of substitutional N (O–Ti–N) and interstitial N (Ti–O–N). DRS exhibited that the light absorption edge red-shifted to visible region. The enhanced visible light photocatalytic activity for the degradation of RhB was mainly attributed to the smaller crystal size, more surface hydroxyl groups, stronger light absorption in visible region and narrower band gap energy.

© 2012 Production and hosting by Elsevier B.V. on behalf of King Saud University. This is an open access article under the CC BY-NC-ND license (<http://creativecommons.org/licenses/by-nc-nd/3.0/>).

1. Introduction

During the past decades, the application of titanium dioxide (TiO₂) photocatalyst for degradation of pollutants has been extensively studied. However, the main drawback was that pure TiO₂ can only be activated under UV light irradiation because of its large band gap energy (~3.2 eV) (Bosc et al., 2003). Thus, in order to extend the light absorption edge to visible region, many attempts have been made (Sato, 1986; Kohtani et al., 1993; Sun et al., 2003). Recently, TiO₂ doped with non-metal element, such as N, C, F, B and S, was proved

* Corresponding author at: Department of Environmental Science and Engineering, Heilongjiang University, Harbin, Heilongjiang Province, PR China. Tel.: +86 451 86608549; fax: +86 451 86413259. E-mail address: yuxjuan@hit.edu.cn (X. Yu).

Peer review under responsibility of King Saud University.



Production and hosting by Elsevier

to be an effective approach to enhance the photoresponse and visible light photoactivity (Asahi et al., 2001; Sakthivel and Kisch, 2003; Zhao et al., 2004; Ohno et al., 2003; Yamaki et al., 2003). Among which, TiO₂ doped with N has been considered as one of the most effective approach to improve the photocatalytic activity of TiO₂ in visible light region (Diwald et al., 2004).

In this work, a series of N doped TiO₂ nanoparticles were synthesized using ammonia chloride as nitrogen source. The resulting materials were characterized by XRD, TEM, SEM, Raman, XPS, FT-IR and DRS. In addition, the photocatalytic activity of the as-synthesized samples was evaluated by the degradation of rhodamine B (RhB) under visible light irradiation.

2. Experimental

All the chemicals used in this work were of analytic grade and were employed without further purification, and doubly deionized water (DI) was used throughout.

2.1. Synthesis of materials

TiO₂-based photocatalysts were synthesized by sol-gel method. In a typical process, 10 mL of tetrabutyl titanate was dissolved in 40 mL of anhydrous ethanol to produce Ti(OBu)₄-C₂H₅OH solution. Meanwhile, 12 mL of dilute nitric acid (1:5, volume ratio between nitric acid and deionized water) and a certain amount of ammonium chloride were added to another 10 mL of anhydrous ethanol in turn to form C₂H₅OH-HNO₃-water solution. Next, the C₂H₅OH-HNO₃ solution was slowly added dropwise to the Ti(OBu)₄-C₂H₅OH solution under vigorous stirring to carry out a hydrolysis. Then, the obtained yellowish transparent sol was aged for 6 h after continuously stirring for 2 h. Subsequently, the resulting yellowish transparent sol was dried for 36 h in an oven at 80 °C, and then calcined for 4 h at a certain temperature with a heating rate of 3 °C min⁻¹. Finally, the TiO₂-based photocatalysts were successfully obtained.

Through changing the weight content of ammonium chloride and calcination temperature, a series of nitrogen doped TiO₂ nanoparticles were synthesized. They were denoted as N_x-TiO₂-T, where “x” and “T” represents the N/Ti molar ratio percent (x = 0, 1, 2, 3, 4, 5) and calcination temperature (T = 350, 400, 450, 500, 550 °C), respectively.

2.2. Characterization of materials

X-ray powder diffraction (XRD) analysis was carried out with a Rigaku D/max III apparatus using Cu K α radiation ($\lambda = 0.15406$ nm), operated at 40 kV and 30 mA. Raman spectra were carried out on a Jobin Yvon HR800 Raman spectrophotometer (equipped with Ar laser excitation wavelength of 457.9 nm) to investigate the microstructural and surface stoichiometric information of the samples. Scanning electron microscopy (SEM) and Transmission electron microscopy (TEM) measurements were performed on S-4800 HITACHI SEM and JEOL TEM-3010 electron microscopy instrument, respectively. X-ray photoelectron spectroscopy (XPS) measurements were performed on a PHI-5700 XPS system with a monochromatic Al K α source and a charge neutralizer. All

the binding energies were calibrated to the C1s peak at 284.6 eV of the surface adventitious carbon. Fourier transform infrared spectra (FT-IR) were recorded in a Perkin Elmer Spectrum One system. UV-vis diffuse reflectance spectra (DRS) were determined by a UV-vis spectrophotometer (Shimadzu UV-2550).

2.3. Evaluation of photocatalytic activity

The activities of the as-synthesized catalysts were evaluated by the photocatalytic degradation of RhB solution. The experiments were carried out in a 100 mL of photochemical glass reactor, and a 350 W spherical xenon lamp with a cutoff filter ($\lambda \geq 420$ nm) as a visible-light source were placed at about 20 cm from the photoreactor. In each run, 20 mg TiO₂-based photocatalyst was added into 20 mL RhB solution of 10 mg L⁻¹. Prior to irradiation, the suspension was kept in the dark under stirring for 30 min to ensure the establishing of an adsorption/desorption equilibrium. At given time intervals, the collected samples after centrifugation and filtration were measured by a T6 UV-vis spectrometer to determine the concentration of RhB solution.

3. Results and discussion

3.1. Measurements of XRD and Raman

TiO₂ usually exists in two main crystallographic form, anatase (A) and rutile (R). The XRD peaks at $2\theta = 25.3^\circ$ (101) and $2\theta = 27.4^\circ$ (110) are often taken as the characteristic peaks of anatase and rutile crystal phase, respectively. The crystallite size can be determined from the broadening of corresponding X-ray spectral peak by Scherrer formula (Zhang et al., 2000): $d = \frac{k\lambda}{\beta \cos \theta}$, where d is the crystallite size, λ is the wavelength of the X-ray radiation (in our test, $\lambda = 0.15406$ nm), k is usually taken as 0.89, and β is the line width at half-maximum height of the main intensity peak after subtraction of the equipment broadening. Meanwhile, the percentage of anatase in the TiO₂ samples can also be estimated from the respective integrated characteristic XRD peak intensities using the quality factor ratio of anatase to rutile (1.265). Fig. 1 showed the

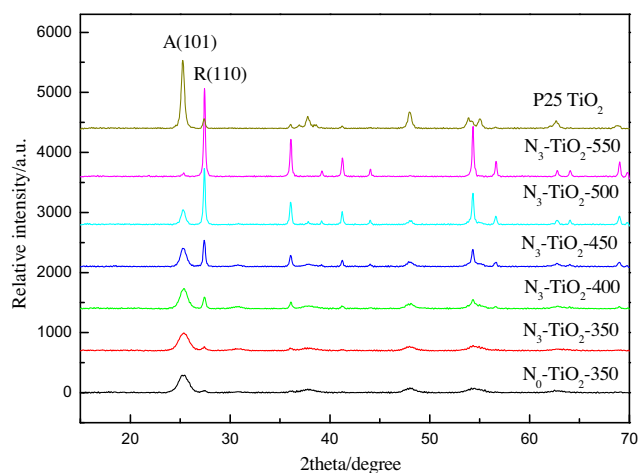


Figure 1 XRD patterns of pure TiO₂ and N₃-TiO₂ catalysts calcined at different temperature.

XRD patterns of pure TiO_2 and $\text{N}_3\text{-TiO}_2$ calcination at different temperature. From Fig. 1, it can be seen that as the thermal treatment temperature increased, the XRD peak width of anatase phase at $2\theta = 25.3^\circ$ gradually became sharper, indicating that the crystallite size gradually became larger. As expected, compared with the pure TiO_2 , $\text{N}_3\text{-TiO}_2$ did not exhibit any new XRD peak, indicating that no new phase appeared. For the samples calcination at 350°C , the as-synthesized $\text{N}_3\text{-TiO}_2$ nanoparticle with about 5 nm anatase crystallite sizes has a mixed phase composition of 80% anatase and 20% rutile, whose phase composition was similar to that of the internationally commercial P25 TiO_2 . The P25 usually exhibits high photocatalytic activity, which is commonly recognized to be due to its mixed phase composition. Thus, it can be predicted that the as-prepared $\text{N}_3\text{-TiO}_2\text{-350}$ should possess excellent photocatalytic activity because of its mixed phase composition.

Raman spectroscopy is a powerful technique for characterizing the microstructural and surface stoichiometric information of inorganic oxide. In the Raman spectrum of TiO_2 , the peaks positioned at 147, 197, 396, 514, and 636 cm^{-1} corresponding to $\text{A}_{1g} + 2\text{B}_{1g} + 3\text{E}_g$ modes demonstrated the presence of anatase phase, while other peaks, located at 235, 443 and 608 cm^{-1} , are characteristic of the rutile phase (Tian et al., 2008; Ohsaka et al., 1978). Fig. 2 showed the Raman spectra of the pure and $\text{N}_3\text{-TiO}_2\text{-350}$ samples. It can be confirmed that the two TiO_2 samples had similar phase composition, both possessing a main anatase phase composition with a small amount of rutile, which was consistent with the XRD characterization. Further, a significant red shift (toward the low wavenumber region) and a little small full-width at half maximum (FWHM) at 147 cm^{-1} can be observed for the $\text{N}_3\text{-TiO}_2$ sample from the insert pattern of Fig. 2, predominantly for the main peak around 147 cm^{-1} from 150.6 to 145.3 cm^{-1} . It has been known that the shift of the peak positions and the changes of the width related to changes of surface oxygen deficiency (Zhou et al., 2006). The blue shift and decrease in peak broadening demonstrated that the content of oxygen deficiency increased, which might be attributed to the formation of high crystallinity and N doping.

3.2. SEM and TEM Measurements

Fig. 3 showed the SEM and TEM photographs of $\text{N}_3\text{-TiO}_2\text{-350}$ nanoparticles. It can be seen that there were many

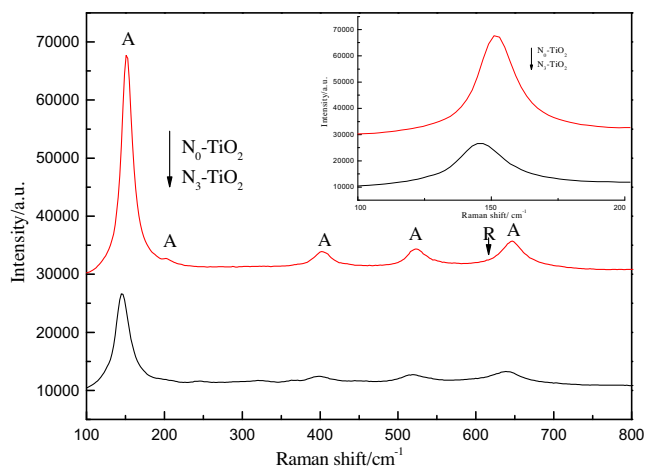


Figure 2 Raman spectra of pure and N doped TiO_2 samples.

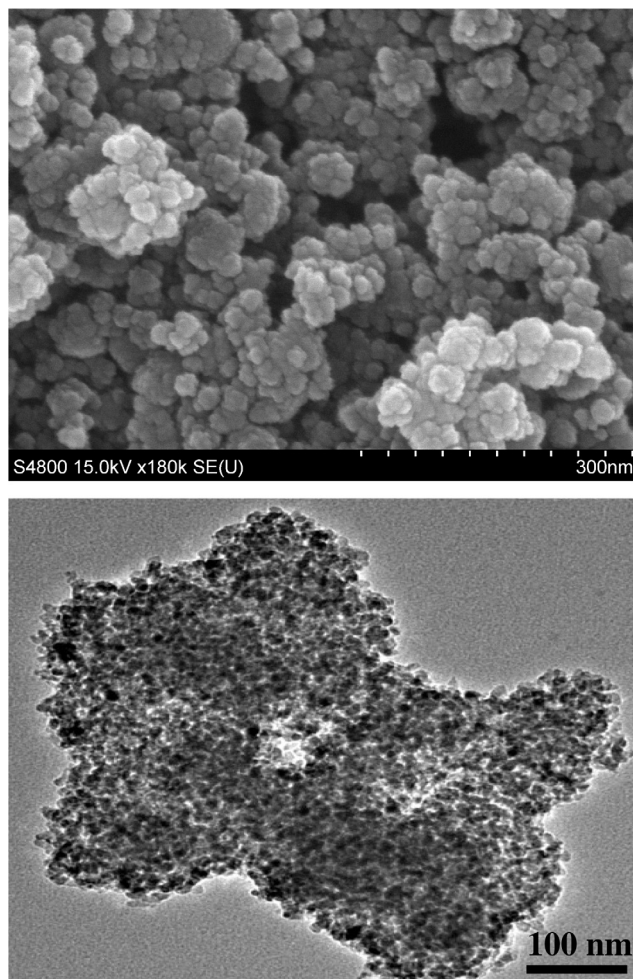


Figure 3 SEM (a) and TEM (b) photographs of $\text{N}_3\text{-TiO}_2\text{-350}$.

sphere-like nanoparticles with various caves and heaves, which mainly resulted from the aggregates of nanocrystalline TiO_2 . As shown in Fig. 3b, $\text{N}_3\text{-TiO}_2$ sample displayed sphere, with average particle size of about 5 nm, which was in accordance with the XRD characterization. In addition, slight agglomeration was also observed.

3.3. Measurements of XPS and FT-IR

XPS analysis was performed in order to investigate the chemical composition and chemical state of the as-synthesized $\text{N}_3\text{-TiO}_2$. Fig. 4A showed a comparison of the XPS survey spectra of pure TiO_2 and $\text{N}_3\text{-TiO}_2$ samples, respectively. For pure TiO_2 sample, it only contained C, O and Ti elements, and the atomic composition of C, O, and Ti elements were 21.05, 56.35, and 22.60 at.%, respectively. On the contrary, the $\text{N}_3\text{-TiO}_2$ sample not only contained C, O and Ti elements, but also a small amount of atomic N, which probably came from the dopants during the calcination. The atomic compositions of C, O, Ti and N elements were 20.98, 55.47, 22.59 and 0.96 at.%, respectively.

In order to investigate the chemical state of N atom in the as-synthesized samples, the N1s core level of $\text{N}_3\text{-TiO}_2\text{-350}$ was analyzed with XPS. As shown in Fig. 4B, two N1s XPS peaks

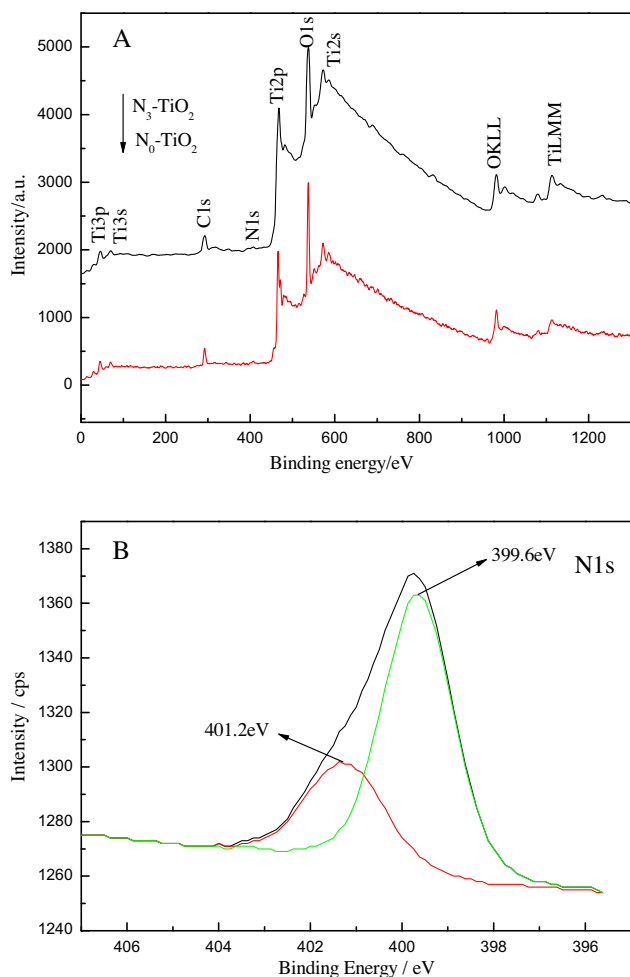


Figure 4 Global XPS of the as-prepared TiO₂ (A) and N1s spectra for N₃-TiO₂ photocatalyst (B).

were presented at 401.2 and 399.6 eV, respectively. The first peak at binding energy of 401.2 eV was assigned to the presence of oxidized nitrogen such as Ti–O–N (Han and Bai, 2009), while the latter peak was attributed to anionic N⁻ in the form of N–Ti–O bond (Xu et al., 2008). However, there was no typical indication of Ti–N bond formation. By comparing with the typical binding energy of 396 eV in Ti–N (Asahi et al., 2001), the latter peak was 3.6 eV higher, which was ascribed to the lower electron density of TiO₂ when N atom substituted for O atom. Therefore, it was clear that N–Ti–O and Ti–O–N coexist in N₃-TiO₂ nanoparticles.

FT-IR spectra of as-synthesized pure and N₃-TiO₂-350 nanoparticles were shown in Fig. 5. Clearly, both of the samples exhibited similar vibrations in the IR region. The intensive and broad band at low wavenumber range between 400 and 800 cm⁻¹ were ascribed to the strong stretching vibrations of Ti–O and Ti–O–Ti bonds (Yu et al., 2003). Two peaks located at 3400 and 1620 cm⁻¹ were assigned to the stretching vibration of hydroxyl group on the surface and O–H bending of dissociated or molecularly adsorbed water molecules, respectively (Ren et al., 2007; Wang et al., 2007). Noticeably, compared with that in pure TiO₂, the intensity of the two absorption bands in the as-synthesized N₃-TiO₂-350 was stronger. This

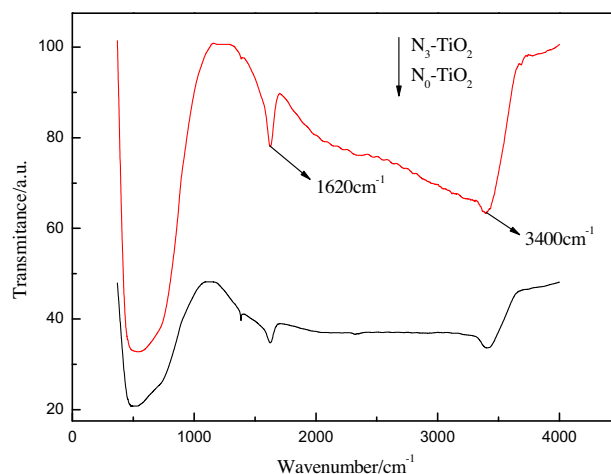


Figure 5 FT-IR spectra for as-prepared pure and N₃-TiO₂ photocatalyst.

indicated that the N₃-TiO₂ sample had more surface-adsorbed water and hydroxyl groups, which played an important role in the photocatalytic reaction. On the one hand, the hydroxyl groups can capture the photo-induced holes (h⁺) when irradiated with light and then form hydroxyl radicals (·OH) with high oxidation capability. On the other hand, the surface hydroxyl groups can also act as absorption centers for O₂ molecules and finally form hydroxyl radicals to enhance the photocatalytic activity.

3.4. UV–vis DRS

The UV–vis diffuse reflectance spectra of the as-synthesized pure and N₃-TiO₂-350 samples were shown in Fig. 6. As a comparison, the spectrum of P25 TiO₂ was also measured and shown in Fig. 6. Obviously, it can be observed that the UV–vis adsorption edge of pure TiO₂ was similar to that of P25 TiO₂, though N₃-TiO₂ shifted to the visible-light region and the optical band edge exhibited a remarkable red-shift with respect to that of pure TiO₂. Furthermore, N₃-TiO₂ sample had two characteristic light absorption edges. One of them

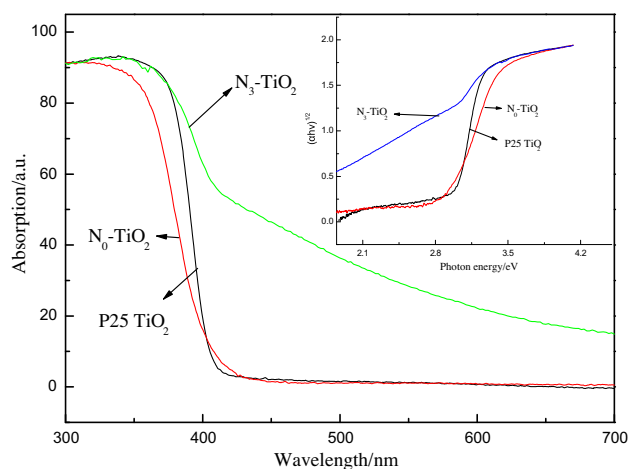


Figure 6 UV–vis diffuse reflectance spectra of the as-prepared pure and N₃-TiO₂ samples.

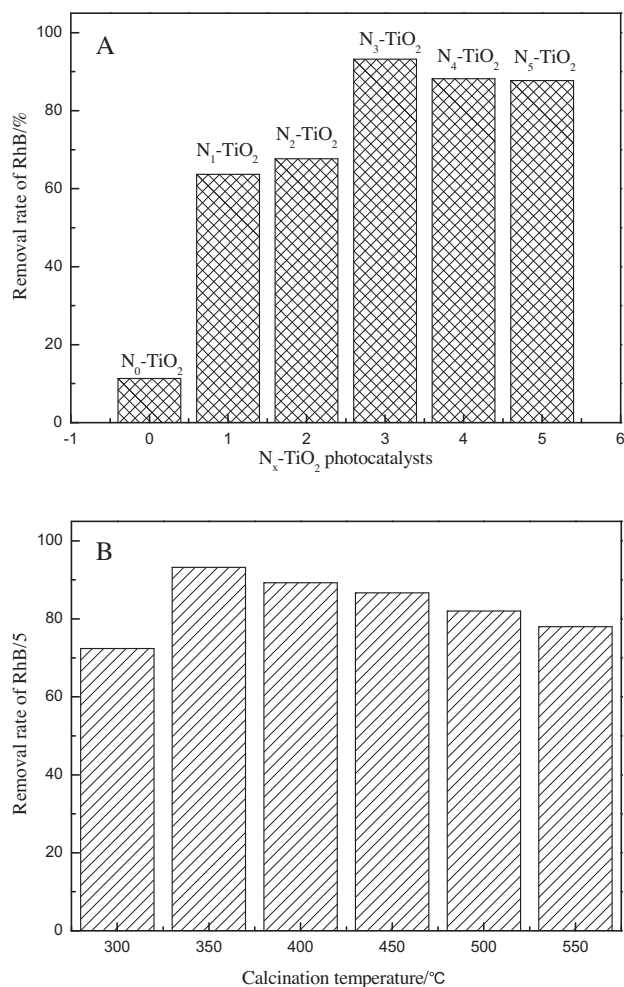


Figure 7 Photoradiation rate of RhB under visible-light irradiation on N_x -TiO₂- T with different N/Ti molar ratio percent (A) and calcination temperature (B).

corresponds to electron promotion from valence band to conduction band while the other originated from the new energy levels in the forbidden band of TiO₂ formed by N-doping. Additionally, the Kubelka–Munk function (Spadavecchia et al., 2010) was used to calculate the band gap energies of the as-synthesized TiO₂ samples by plotting $[F(R) \cdot E]^{1/2}$ versus energy of light and the results were shown in the inset in Fig. 6. The band gap energies were 2.85 and 3.1 eV for N₃-TiO₂ and TiO₂, respectively, revealing that the band gap of TiO₂ was narrowed by N doping. In this work, the band gap narrowing may be caused by the introduction of nitrogen from ammonium chloride into the lattice of TiO₂. Therefore, it can be concluded that the sample of N₃-TiO₂ may exhibit high photocatalytic activity under visible-light irradiation.

3.5. Evaluation of photocatalytic activity

Photocatalytic activities of the N_x -TiO₂- T samples were investigated by photodegradation of RhB under visible-light irradiation. Fig. 7 showed the effects of the ammonium chloride concentration (A) and calcination temperature (B) in the N_x -TiO₂- T samples on the photodegradation of RhB under visible-light irradiation. As expected, N_x -TiO₂ exhibited the

higher visible-light photocatalytic activity due to the effect of N doping into the TiO₂ lattice. It was found in Fig. 7A that N₃-TiO₂ had obviously the highest photocatalytic activity, suggesting that there was an optimum value for the N-doping. The photodegradation rate of RhB increased when doping nitrogen amount increased, and the degradation rate was highest when the amount of dopants reached 3%. Furthermore, increased in the amount of dopants decreased the photodegradation rate. This can be explained by the fact that, when the dopants increased, the number of N atoms replacing the oxygen sites increased. This caused the increase of oxygen vacancy and Ti³⁺, which leading an enhancement of photocatalytic activity. But some oxygen vacancy and Ti³⁺ sites became the recombination centers of photo-induced holes and electrons (h^+/e^-) as the dopants increased continuously, resulting in the decrease of photocatalytic activity accordingly. As seen from Fig. 5B, the optimum calcination temperature was 350 °C. Samples calcined at elevated temperatures showed lower photocatalytic activity due to the loss of the nitrogen dopant and the larger particle size. Therefore, it can be concluded that the N₃-TiO₂-350 sample should show the maximum photocatalytic activity among all the as-synthesized samples, the photodegradation rate of RhB was 90.3% within 120 min, which could be attributed to the mixed phase composition, more surface hydroxyl groups, intense absorption in visible-light region and narrow band gap energy.

4. Conclusions

A series of N doped TiO₂ nanoparticles were successfully synthesized to fabricate the high active photocatalyst under visible-light irradiation. Doping with N could narrow the band gap of TiO₂ and extend the absorption edge to visible-light region due to the fact that the N coexisted in multi-form of substitutional N–Ti–O and Ti–O–N in the forbidden band of TiO₂. The enhanced photocatalytic activity on degradation of RhB under visible-light irradiation was mainly attributed to the mixed phase composition, more surface hydroxyl groups, intense absorption in visible-light region and narrow band gap energy.

Acknowledgments

This work was supported by National Natural Science Foundation of China for Youth (21106035) and Youth Scholar Backbone Supporting Plan Project for general colleges and universities of Heilongjiang province (1151G034).

References

- Asahi, R., Morikawa, T., Ohwaki, T., Aoki, K., Taga, Y., 2001. Visible-light photocatalysis in nitrogen-doped titanium oxides. *Science* 293, 269–271.
- Bosc, F., Ayral, A., Albouy, P.A., Guizard, C., 2003. A simple route for low-temperature synthesis of mesoporous and nanocrystalline anatase thin films. *Chem. Mater.* 15, 2463–2468.
- Diwald, O., Thompson, T.L., Zubkov, T., Goralski, E.G., Walck, S.D., Yates Jr, J.T., 2004. Photochemical activity of nitrogen-doped rutile TiO₂ (1 1 0) in visible light. *J. Chem. B* 108, 6004–6008.

- Han, H., Bai, R.B., 2009. Buoyant photocatalyst with greatly enhanced visible-light activity prepared through a low temperature hydrothermal method. *Ind. Eng. Chem. Res.* 48, 2891–2898.
- Kohtani, S., Kudo, A., Sakata, T., 1993. Spectral sensitization of a TiO₂ semiconductor electrode by CdS microcrystals and its photoelectrochemical properties. *Chem. Phys. Lett.* 206, 166–170.
- Ohno, T., Mitsui, T., Matsumura, M., 2003. Photocatalytic activity of S-doped TiO₂ photocatalyst under visible light. *Chem. Lett.* 32, 364–365.
- Ohsaka, T., Izumi, F., Fujiki, Y., 1978. Raman-spectrum of anatase. TiO₂. *J. Raman Spectrosc.* 7, 321–324.
- Ren, L., Huang, X.T., Sun, F.L., He, X., 2007. Preparation and characterization of doped TiO₂ nano-dandelion. *Mater. Lett.* 61, 427–431.
- Sakthivel, S., Kisch, H., 2003. Daylight photocatalysis by carbon-modified titanium dioxide. *Angew. Chem. Int. Ed.* 42, 4908–4911.
- Sato, S., 1986. Photocatalytic activity of NO_x-doped TiO₂ in the visible light region. *Chem. Phys. Lett.* 123, 126–128.
- Spadavecchia, F., Cappelletti, C., Ardizzone, S., Bianchi, C.L., Cappelli, S., Oliva, C., Scardi, P., Leoni, M., Fermo, P., 2010. Solar photoactivity of nano-N-TiO₂ from tertiary amine: role of defects and paramagnetic species. *Appl. Catal. B: Environ.* 96, 314–322.
- Sun, B., Vorontsov, A.V., Smirniotis, P.G., 2003. Role of platinum deposited on TiO₂ in phenol photocatalytic oxidation. *Langmuir* 19, 3151–3156.
- Tian, G.H., Fu, H.G., Jing, L.Q., Xin, B.F., Pan, Kai, 2008. Preparation and characterization of stable biphasic TiO₂ photocatalyst with high crystallinity, large surface area, and enhanced photoactivity. *J. Phys. Chem. C* 112, 3083–3089.
- Wang, J.W., Zhu, W., Zhang, Y.Q., Liu, S.X., 2007. An efficient two-step technique for nitrogen-doped titanium dioxide synthesizing: visible-light-induced photodecomposition of methylene blue. *J. Phys. Chem. C* 111, 1010–1014.
- Xu, J.H., Li, J.X., Dai, W.L., Cao, Y., Li, H.X., Fan, K.N., 2008. Simple fabrication of twist-like helix N, S-codoped titania photocatalyst with visible-light response. *Appl. Catal. B: Environ.* 79, 72–80.
- Yamaki, T., Umebayashi, T., Sumita, T., Yamamoto, S., Maekawa, M., Kawasuso, A., Itoh, H., 2003. Fluorine-doping in titanium dioxide by ion implantation technique. *Nucl. Instrum. Methods Phys. Res. Sect. B* 206, 254–258.
- Yu, J.G., Yu, H.G., Cheng, B., Zhao, X.J., Yu, J.C., Ho, W.K., 2003. The effect of calcination temperature on the surface microstructure and photocatalytic activity of TiO₂ thin films prepared by liquid phase deposition. *J. Phys. Chem. B* 107, 13871–13879.
- Zhang, Q.H., Gao, L., Guo, J.K., 2000. Effects of calcination on the photocatalytic properties of nanosized TiO₂ powders prepared by TiCl₄ hydrolysis. *Appl. Catal. B: Environ.* 26, 207–215.
- Zhao, W., Ma, W.H., Chen, C.C., Zhao, J.C., Shuai, Z.G., 2004. Efficient degradation of toxic organic pollutants with Ni₂O₃/TiO_{2-x}B_x under visible irradiation. *J. Am. Chem. Soc.* 126, 4782–4783.
- Zhou, J.K., Zhang, Y.X., Zhao, X.S., Ray, A.K., 2006. Photodegradation of benzoic acid over metal-doped TiO₂. *Ind. Eng. Chem. Res.* 45, 3503–3511.